

# Introducing strong correlation effects into graphene by gadolinium intercalation

S. Link,<sup>1</sup> S. Forti,<sup>1,\*</sup> A. Stöhr,<sup>1</sup> K. Küster,<sup>1</sup> M. Rösner,<sup>2,3,4</sup> D. Hirschmeier,<sup>5</sup> C. Chen,<sup>6</sup> J. Avila,<sup>6</sup> M.C. Asensio,<sup>7</sup> A.A. Zakharov,<sup>8</sup> T.O. Wehling,<sup>2</sup> A.I. Lichtenstein,<sup>5</sup> M.I. Katsnelson,<sup>4</sup> and U. Starke<sup>1,†</sup>

<sup>1</sup>*Max-Planck-Institut für Festkörperforschung, Heisenbergstr. 1, D-70569 Stuttgart, Germany*

<sup>2</sup>*Institute for Theoretical Physics, Bremen Center for Computational Materials Science, University of Bremen Otto-Hahn-Allee 1, 28359 Bremen, Germany*

<sup>3</sup>*Department of Physics and Astronomy, University of Southern California, Los Angeles, CA 90089-0484, USA*

<sup>4</sup>*Radboud University, Institute for Molecules & Materials, Heijendaalseweg 135, 6525 AJ Nijmegen, Netherlands*

<sup>5</sup>*Universität Hamburg, Institut für Theoretische Physik, D-20355 Hamburg, Germany*

<sup>6</sup>*Synchrotron SOLEIL and Université Paris Saclay, Orme des Merisiers, Saint-Aubin-BP 48, 91192 Gif sur Yvette, France*

<sup>7</sup>*Madrid Institute of Materials Science (ICMM), Spanish Scientific Research Council (CSIC), Cantoblanco, E-28049 Madrid - SPAIN*

<sup>8</sup>*MAX IV Laboratory, Lund University, Fotogatan 2, 22484 Lund, Sweden*

(Dated: September 19, 2019)

Exotic ordered ground states driven by electronic correlations are expected to be induced in monolayer graphene when doped to the Van Hove singularity. Such doping levels are reached by intercalating Gd in graphene on SiC(0001), resulting in a strong homogeneity and stability. The electronic spectrum now exhibits severe renormalizations. Flat bands develop which is driven by electronic correlations according to our theoretical studies. Due to strong electron-phonon coupling in this regime, polaron replica bands develop. Thus, interesting ordered ground states should be made accessible.

PACS numbers:

Monolayer graphene can be viewed as prototype of the materials' class of Dirac materials [1–4]. At low carrier concentrations, the low energy excitations can be described as massless Dirac Fermions, as the electronic spectrum is nominally linear in a single particle picture, resulting in a conical shape at the high symmetry points  $\bar{K}$  and  $\bar{K}'$  of graphene's Brillouin zone (BZ) (see Fig. 1 (a)). However, when including many body interactions, especially electronic correlations, the bands can be reshaped drastically, due to the strong onsite Coulomb repulsion in graphitic systems [5]. Furthermore, long range electronic correlations are substantial in this system due to its two-dimensionality and Dirac-like spectrum [6, 7]. At low doping levels, this results in logarithmic corrections in the electronic spectrum [8, 9]. At finite n-type doping levels, the total band width of the  $\pi$  band structure gets significantly lowered [10]. In the extreme case of high doping, a Van Hove singularity (VHs) in the density of states is reached, whereas flat bands develop at the Fermi level ( $E_F$ ), connecting  $\bar{K}$  and  $\bar{K}'$  [11]. Similar effects were observed in strongly correlated materials like cuprates [12] and ruthenates [13], referred to as extended Van Hove singularities (eVHs) [14–17]. In the case of cuprates, this then called Van Hove (VH) scenario appears to be partially connected to the rich and unusual physical phenomena and to the different phases found in those materials [18]. Despite the fundamental differences to these systems, one might expect to find similarly rich physics in graphene in this regime. Generically, the emergence of an eVHs is a hallmark of a non-Fermi liquid

state of matter called Fermi condensate [14–17] where the electronic dispersion becomes flat at the chemical potential in a finite momentum interval  $k_1 < |k| < k_2$ , i.e.  $e_k = \mu$  for  $T \rightarrow 0$ . In this light, it is especially interesting to draw the connection to predictions of exotic ordered ground states in graphene at VH-filling, like chiral superconductivity driven by repulsive electron-electron interaction [19, 20], where such strong band renormalizations are not taken into account.

In order to experimentally reach the VHs in graphene, extreme carrier induction is required which can only be achieved by chemical doping. For this purpose a combination of adsorption and intercalation of Ca and K was applied before [11], where the surface exposure and reactivity of dopants cause severe limitations in thermal and chemical stability. Intercalation alone, however, i.e., the full insertion of the dopant between graphene and its substrate assures a physical (and chemical) protection by the covering graphene layer [21, 22]. Thus, detailed in-situ band structure analysis [23], characterization with ex-situ techniques [22] or further processing into a device are then possible [24]. Indeed, transfer and contacting under Ar atmosphere allows the application of cryogenic transport experiments, as currently underway.

Accordingly, here we intercalate Gd atoms beneath the so called zero-layer graphene (ZLG) on SiC(0001) [25]. Intercalation was performed by depositing Gd from an e-beam evaporator combined with heating up to temperatures of 1200 °C. The Gd-intercalated graphene is thermally stable and sufficiently doped to provide VH-

filling. The intercalation geometry (see Fig. 1 (b)) provides chemical stability, such that no degeneration in the samples could be observed within weeks, when kept under ultra-high vacuum conditions ( $p < 1 \times 10^{-8}$  mbar) in contrast to ref. 11 where doping from both sides makes the system severely environment sensitive. Low energy electron microscopy (LEEM) experiments prove the homogeneity on a mesoscopic scale [25]. LEEM as well as X-ray photoelectron spectroscopy (XPS) were carried out at beamline I311 of MAX-lab synchrotron, Lund (Sweden). The stability supports high quality band structure measurements using angle-resolved photoelectron spectroscopy (ARPES) which was conducted at beamline ANTARES of SOLEIL synchrotron (France), at Bessy II beamline UE112 of Helmholtz Zentrum Berlin and at beamline I4 of MAX-Lab.

The experimental results are simulated by band modeling within density functional theory (DFT) for Gd adsorbed on graphene [25], which can reproduce the observed doping levels, yet cannot account for the strong renormalizations found in the experiment. The DFT calculations were performed within the generalized gradient approximation (GGA) [26] using the Vienna Ab Initio Simulation Package (VASP) [27] and the projector augmented wave (PAW) [28, 29] basis sets. To overcome the limitations of DFT based mean field techniques, we utilize the Hubbard model, which is solved in fluctuating exchange approximation (FLEX) [25, 30]. Introducing the effects of spin fluctuations, we could reproduce the experimental results. The temperature was chosen to be  $T = 33$  meV (386 K) in all calculations.

Fig. 1(c) displays the result of ARPES measurements of Gd intercalated ZLG on SiC(0001) spanning a cut from  $\bar{K}$  over  $\bar{M}$  to  $\bar{K}'$  [25, 31]. Around  $\bar{K}$ , the conical  $\pi$  band of monolayer graphene emerges, which proves successful intercalation [21, 25]. In contrast to other intercalants, Gd produces graphene with an extremely high n-type doping level. The Dirac point is shifted by about 1.6 eV from  $E_F$  to higher binding energy. This is sufficient to reach the saddle point at  $\bar{M}$ , as seen by the strong spectral weight at  $\bar{M}$  near  $E_F$  – now by intercalation alone. Concomitantly, the Fermi surface (FS) experiences a Lifshitz transition, cf. Fig. 1(d). Instead of two electron pockets, centered around  $\bar{K}$  and  $\bar{K}'$ , one giant hole pocket emerges around  $\bar{\Gamma}$ . From an experimental fit to the FS, one can directly calculate a filling of about 0.12 in the  $\pi^*$  band following Luttinger’s theorem [32]. This corresponds to about  $4.5 \times 10^{14}/\text{cm}^2$  additional electrons compared to neutral graphene [33]. In view of a single electron picture (nearest-neighbor tight-binding, NN-TB), this would not be sufficient to reach the VH-filling. There the transition should be at 1/4 filling or  $9.5 \times 10^{14}/\text{cm}^2$  electron density. Further differences can be seen in the dispersion in Fig. 1(c). While the bands along the  $\bar{\Gamma}\bar{K}$ -direction can be fitted well with NN-TB bands with a reasonable hopping parameter of 3.1 eV, the bands along the  $\bar{K}\bar{M}$ -

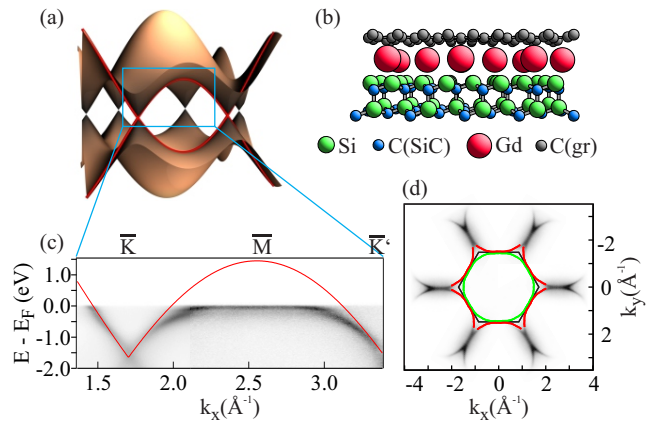


FIG. 1: ARPES on Gd intercalated ZLG: (a) Illustration of graphene’s  $\pi$  bands. (b) Side view model of the intercalation system. (c) Two concatenated ARPES measurements cutting from  $\bar{K}$  over  $\bar{M}$  to  $\bar{K}'$  together with a band modeled with NN-TB (red trace). The left part (below  $2.1 \text{ \AA}^{-1}$ ) was taken with 30 eV and the right part (above  $2.1 \text{ \AA}^{-1}$ ) with 100 eV photon energy. (d) Symmetrized FS taken with 90 eV photon energy together with its experimental fit (red and green lines). The black hexagon represents graphene’s first BZ.

direction deviate strongly. Near  $\bar{K}$  the band velocity is already drastically reduced, whilst around  $\bar{M}$  the band is completely flat over a range of about  $1 \text{ \AA}^{-1}$  with renormalizations on the order of 1.5 eV as compared to the NN-TB model (red trace in the figure). Optical absorp-

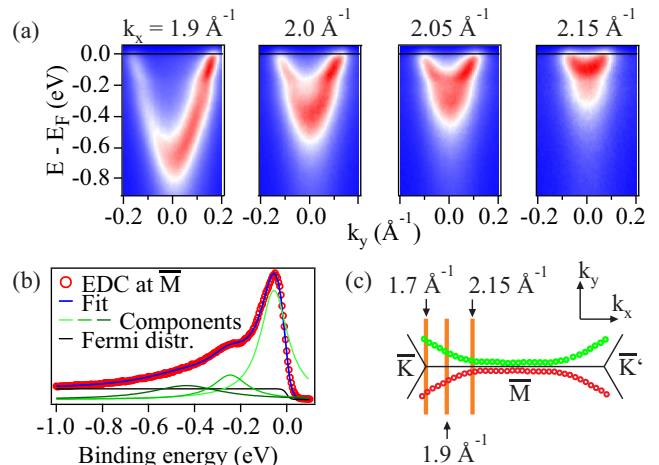


FIG. 2: Electron-phonon coupling around  $\bar{M}$ : (a) Series of ARPES cuts taken perpendicular to the  $\bar{K}\bar{M}$ -direction at different  $k_x$ , as indicated in panel (c), photon energy 35 eV. (b) EDC at  $\bar{M}$  together with a fit of 3 equidistant Lorentzians multiplied with the Fermi distribution. (c) Fitted FS around  $\bar{M}$ , illustrating the parallel sections of the FS.

tion experiments taken on doped graphene [34] revealed the saddle point at  $\bar{M}$  also at significantly lower binding energy compared to NN-TB. The binding energy reduc-

tion increased with the doping level, which was associated with electron-electron interaction. However, the situation in these experiments is still distinctly different from a flat band near  $\bar{M}$ , which cannot be accounted for by any smooth modification to NN-TB.

As apparent in Fig. 1(c), the flat band at  $\bar{M}$  is accompanied by a second band at higher binding energy, as also observed in ref. [11]. This spectral feature can be associated with electron-boson coupling, as illustrated further in Fig. 2(a) by spectral cuts taken perpendicular to the cut in Fig. 1(c), revealing the spectral evolution from  $\bar{K}$  towards  $\bar{M}$  of the typical kink structure near  $E_F$ , induced by phonon coupling. At about  $k_x=2 \text{ \AA}^{-1}$ , the kink structure evolves smoothly into a structure, where a sharp coherent branch near  $E_F$  is replicated by a broader incoherent part at higher binding energy (second band). Taking an energy distribution curve (EDC) from  $\bar{M}$  (see Fig. 2(b)), the distribution can be fitted by three Lorentzians with a mutual distance of 190 meV. This energy corresponds to graphene's in-plane optical phonon modes at  $\bar{\Gamma}$ . The observed spectral feature is thus likely associated with the formation of polarons as new electron-phonon composite quasiparticles [35]. From the spectral fraction of the coherent part near  $E_F$  of 0.6, one can estimate the coupling constant  $\alpha$  to this particular phonon mode to be on the order of 1 by comparing to diagrammatic Monte-Carlo simulations [35]. This is strongly enhanced compared to coupling constants to this phonon mode in graphene, which is not in the eVHs regime [36]. A detailed, zoomed view of the FS, cf. Fig. 2(c), demonstrates that the sector at  $\bar{M}$  is very straight and thereby nested to its counterpart in the repeated BZ. Generally, this condition strongly enhances resonant coupling, as the phase space for phonon scattering within these sections of the FS is enhanced. As the two FS sections are very close, the corresponding phonons have about zero momentum, i.e. they are located around  $\bar{\Gamma}$  in the BZ. The previously extracted energy of the phonon mode is in agreement with this picture. These phonon-induced spectral features may have a strong influence on or even enhance the observed flat band section. However, with reasonable coupling constants, this effect alone cannot induce the flat band.

In order to provide information about interface structure and chemistry, low-energy electron diffraction (LEED) and XPS experiments were conducted. Fig. 3(a) displays two LEED patterns taken with different electron energies. As expected for intercalated ZLG, none of the reconstruction spots associated with the pristine ZLG structure are visible, since the covalent bonding to the substrate in the pristine ZLG system is lifted. Instead, the first order  $(1 \times 1)$ -spots of graphene emerge sharp and bright (67.5 eV pattern). Besides, a new periodicity can be recognized. As apparent in the 30 eV pattern by the marked  $(\frac{1}{3}, \frac{1}{3})$ -spots, this periodicity is based on a  $(\sqrt{3} \times \sqrt{3})R30^\circ$  superstructure with respect

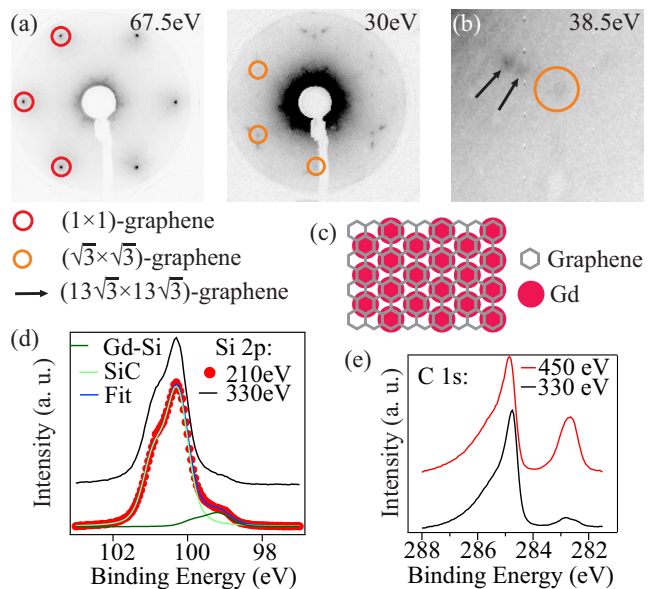


FIG. 3: LEED and XPS on Gd intercalated ZLG: (a) LEED patterns taken with two different electron energies. (b) Diffraction pattern closeup around a graphene  $(\frac{1}{3}, \frac{1}{3})$ -spot. The different spots in (a,b,c) are ascribed in the legend. (c) Sketch of a simplified Gd- $(\sqrt{3} \times \sqrt{3})R30^\circ$ -graphene structure. (d) Si 2p spectra of Gd intercalated ZLG taken with two different photon energies together with a fit of the two involved chemical species. (e) C 1s spectra of Gd intercalated ZLG taken with two different photon energies.

to graphene. Since the  $(\sqrt{3} \times \sqrt{3})R30^\circ$ -graphene is not part of the total periodicity of the initial ZLG system ( $(13 \times 13)$ -graphene), we conclude that the intercalated Gd primarily arranges with respect to the graphene. Note that the amount of deposited and intercalated Gd, i.e. 0.75-0.8 monolayer of Gd [37], corresponds to a simple  $(\sqrt{3} \times \sqrt{3})R30^\circ$ -graphene structure, as sketched in Fig. 3(c). Yet, it is apparent especially from the elongated spots around the  $(\frac{1}{3}, \frac{1}{3})$ -spots, that this structure itself is reconstructed. In fact, the elongated features around the  $(\frac{1}{3}, \frac{1}{3})$ -spots are two very close spots, as seen in the closeup in Fig. 3(b). Also, an apparent threefold symmetry in the varying intensity of these  $(\frac{1}{3}, \frac{1}{3})$ -spots can be recognized which cannot be explained by the Gd-graphene slab alone.

It is intuitive to explain these modifications by the influence of the substrate in the form of a bonding of the Gd to the topmost Si of the SiC(0001) surface. This is corroborated by the fact that in the Si 2p spectra in XPS (see Fig. 3(d)), two different chemical species of Si can be distinguished. Varying the photon energy and thereby surface sensitivity shows that the doublet around 100.5 eV has to be associated with Si in the bulk SiC and that at about 99 eV with Si at the SiC surface, since the latter is more pronounced in the more surface sensitive probe (210 eV photon energy). The strong energy shift

gives evidence for a charge transfer and thus for a bonding to Gd. By comparing the intensity ratio of the two chemical species (5:95) to the case of H-intercalated ZLG (1:2) [21], where every Si on the surface is passivated by one H atom, it can be inferred that only about 3/20 of the Si atoms are passivated in the Gd case. Taking into account the amount of intercalated Gd and the assumption that only one Gd atom is bound to a Si atom respectively, one can estimate, that about 1/3 of the Gd atoms bind to Si. Connecting these results further to the observations made with LEED, the partial bonding explains the apparent threefold symmetry, which originates from the stacking order of the 6H-SiC substrate. Also, as the total periodicity of the graphene-SiC system is a  $(13 \times 13)$ -graphene, one can expect for the total system a  $(\sqrt{3} \times \sqrt{3})R30^\circ$ -superstructure on the  $(13 \times 13)$ -graphene, i.e. a  $(13\sqrt{3} \times 13\sqrt{3})R30^\circ$ -graphene. Indeed, this model captures all the observed diffraction spots.

Concerning the chemistry within the graphene layer, Fig. 3(e) displays C 1s spectra taken with two different photon energies. Two prominent main features can be determined, that must be associated with bulk SiC around 282.5 eV and the graphene between 284.5 eV and 288 eV since in the more bulk sensitive probe (450 eV photon energy), the 282.5 eV binding energy component is clearly more pronounced. In contrast to the low doped case, the C 1s component of graphene does not follow a simple asymmetric distribution that can be simulated by a Doniach Sunjic function, which is often suitable for metals. This is apparent in the clear hump at about 285.8 eV binding energy. Simulations in ref. [38] and also experimental work in ref. [39] for highly doped graphene corroborate our findings. The characteristic shape is meant to be induced by energy loss primarily due to plasmon creation during the photoemission process.

In order to reveal the mechanism responsible for the flat band formation, we performed DFT simulations of Gd adsorbed on graphene in the  $(\sqrt{3} \times \sqrt{3})R30^\circ$  structure sketched in Fig. 3(c) and calculated the unfolded band structure. The results shown in Fig. 4(a) reveal an essentially intact graphene Dirac point, located approximately 1.5 eV below  $E_F$ , which is in line with our ARPES experiments. Hybridization with Gd bands pushes graphene's  $\pi$  bands at  $\bar{M}$  more than 0.5 eV below  $E_F$  and induces a spin-splitting of about 0.5 eV. While a downward shift of the bands at  $\bar{M}$  as compared to NN-TB is in line with our experimental observation, the magnitude of the shift in DFT largely exceeds the experimental one. In particular, there is no pinning of any flat band to  $E_F$  in the  $\bar{K}$ - $\bar{M}$  direction in the DFT results. Indeed, such pinning is a typical hallmark of dynamic electron correlation effects [17], which are beyond DFT based mean field theories. To investigate whether these electronic correlations in form of spin-fluctuations can be responsible for the flattening of the bands along  $\bar{K}$ - $\bar{M}$ , we considered the

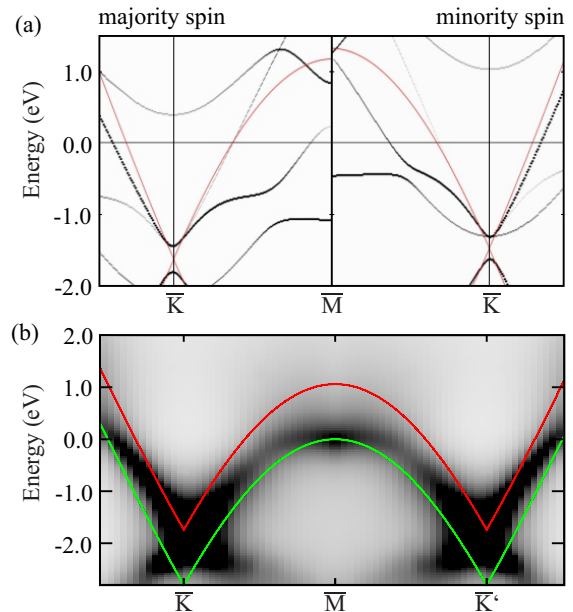


FIG. 4: (a) DFT band structure of Gd on graphene in the  $(\sqrt{3} \times \sqrt{3})R30^\circ$  structure unfolded to the BZ of the primitive graphene unit cell (gray lines) and NN-TB band structure (red). The line thickness of the unfolded bands serves as an approximate measure of an intensity expected in an ARPES experiment. Precisely, the line thickness at some wave vector  $k$  from the BZ of the original graphene lattice indicates the overlap of the corresponding state in the  $(\sqrt{3} \times \sqrt{3})R30^\circ$  supercell with a plane wave from the primitive graphene unit cell at wave vector  $k$ . b) Spectral function as obtained from fluctuating exchange approximation theory. The essential features of the ARPES data (eVHs and the energetic shift of the renormalized spectrum at the Dirac point) are well reproduced. Comparison to the NN-TB model at VH-filling (green curve) as well as a NN-TB model fit to the shift at the  $\bar{K}$  point (red) implies that the renormalization is correlation induced.

following Hubbard model

$$H = -t \sum_{\langle i,j \rangle, \sigma} c_{i\sigma}^\dagger c_{j\sigma} - \mu \sum_{i,\sigma} c_{i\sigma}^\dagger c_{i\sigma} + U \sum_i n_{i,\uparrow} n_{i,\downarrow}, \quad (1)$$

where electrons on site  $i$  with spin  $\sigma$  are created (annihilated) by  $c_{i\sigma}^\dagger$  ( $c_{i\sigma}$ ) and the density operator is given by  $n_{i\sigma} = c_{i\sigma}^\dagger c_{i\sigma}$ . The nearest-neighbour hopping amplitude in our model calculations is  $t = 2.8$  eV, while the chemical potential is set to  $\mu = 2.4$  eV and the Hubbard repulsion is chosen to be  $U = 8.4$  eV. We solve this model using the FLEX approximation [30] which introduces the effects of spin fluctuations. The resulting FLEX spectral function is shown in Fig. 4(b). The comparison with a NN-TB model at VH-filling (green curve) clearly shows that the VHs at  $E_F$  is extended to a flat band that almost stretches half way to  $\bar{K}$ . Furthermore, the spectral weight at  $\bar{K}$  is shifted upwards such that the energy difference of the spectrum between  $\bar{K}$  and  $\bar{M}$  is significantly

reduced to  $t/2$  (while it is  $t$  in the non-interacting NN-TB model). This redistribution of spectral weight can not be described by shifted one-particle NN-TB models (compare red and green curves) which suggests that strong electronic correlations in form of spin fluctuations present indeed a possible origin of the eVHs. Like in the ARPES spectral function, there are no severe renormalizations along the  $\bar{\Gamma}$ - $\bar{K}$  path, resulting in a good agreement with the experiment. In contrast to the experimental spectral function we do not see any indications of a second band close to (below)  $E_F$ . The experimentally observed accompanying band is thus indeed arising from electron-phonon interactions and not from interactions with magnetic fluctuations like paramagnons.

In summary, we have shown that by intercalating Gd underneath zero-layer graphene on SiC(0001) the carbon layer can be decoupled from its substrate. Thereby a strongly doped monolayer graphene system is produced, where an eVHs emerges in the spectral function indicating the realization of a Fermi condensate in graphene. By comparing the experimental spectral function to theoretical results from super-cell DFT as well as many-body FLEX calculations, we found that strong electron-electron correlation effects in form of spin-fluctuations can explain the occurrence of the eVHs, while coupling to phonons seems responsible for the replicas of the eVHs bands at higher binding energies.

We have shown that the right choice of intercalant can result in very high thermal and chemical stability with superb crystallinity. Together with the homogeneity on a large scale, this gives the opportunity to study graphene's many-body properties in the eVHs regime in great detail. Our findings enable the stable and precisely controlled functionalization of graphene, driving the confluence of important technological applications with the quest for microscopic mechanisms that control the properties of the material.

We are indebted to MAX-Lab (Lund, Sweden), SOLEIL (Gif-sur-Yvette, France) and BESSY (Berlin, Germany) for allocating synchrotron beamtime and the facility staff for their advice and support. We would like to thank M. Konuma for his help in XPS measurements. In addition, we would like to acknowledge T. Denig for fruitful discussions in the initial stages of the project. This work was supported by the German Research Foundation (DFG) in the framework of the Priority Program 1459, Graphene. Support by the DFG through Sta315/9-1 is acknowledged in addition. M.R. would like to thank the Alexander von Humboldt Foundation for support. A.A.Z. would like to acknowledge support from Siftelsen för Strategisk Forskning (project RMA15-0024). M.I.K. acknowledges financial support by NWO via the Spinoza Prize. Computational resources were provided by the HLRN-Cluster under Project No. hhp00042.

\* present address: Center for Nanotechnology Innovation CNI@NEST, Piazza San Silvestro 12, 56127 Pisa, Italy

† To whom correspondence should be addressed:

Email: u.starke@fkf.mpg.de;

Electronic address: <http://www.fkf.mpg.de/ga>

- [1] K. S. Novoselov, A. K. Geim, S. V. Morozov, D. Jiang, M. I. Katsnelson, I. V. Grigorieva, S. V. Dubonos, and A. A. Firsov, *Nature* **438**, 197 (2005)
- [2] Y. Zhang, Y. Tan, H. Stormer, and P. Kim, *Nature* **438**, 201 (2005)
- [3] A. H. Castro Neto, F. Guinea, N. M. R. Peres, K. S. Novoselov, and A. K. Geim, *Rev. Mod. Phys.* **81**, 109 (2009)
- [4] C. Berger, Z. Song, X. Li, X. Wu, N. Brown, C. Naud, D. Mayou, T. Li, J. Hass, A. N. Marchenkov, E. H. Conrad, P. N. First, and W. A. de Heer, *Science* **312**, 1191 (2006)
- [5] T. O. Wehling, E. Şaşıoğlu, C. Friedrich, A. I. Lichtenstein, M. I. Katsnelson, and S. Blügel, *Phys. Rev. Lett.* **106**, 236805 (2011)
- [6] S. Das Sarma, E. H. Hwang, and W.-K. Tse, *Phys. Rev. B* **75**, 121406 (2007)
- [7] A. Bostwick, T. Ohta, T. Seyller, K. Horn, and E. Rotenberg, *Nat. Phys.* **3**, 36 (2007)
- [8] D. A. Siegel, C.-H. Park, C. Hwang, J. Deslippe, A. V. Fedorov, S. G. Louie, and A. Lanzara, *Proc. Natl. Acad. Sci.* **108**, 11365 (2011)
- [9] D. C. Elias, R. V. Gorbachev, A. S. Mayorov, S. V. Morozov, A. A. Zhukov, P. Blake, L. A. Ponomarenko, I. V. Grigorieva, K. S. Novoselov, F. Guinea, and A. K. Geim, *Nat. Phys.* **7**, 701 (2011)
- [10] S. Ulstrup, M. Schüler, M. Bianchi, F. Fromm, C. Raidel, T. Seyller, T. Wehling, and P. Hofmann, *Phys. Rev. B* **94**, 081403 (2016)
- [11] J. L. McChesney, A. Bostwick, T. Ohta, T. Seyller, K. Horn, J. González, and E. Rotenberg, *Phys. Rev. Lett.* **104**, 136803 (2010)
- [12] K. Gofron, J. C. Campuzano, A. A. Abrikosov, M. Lindroos, A. Bansil, H. Ding, D. Koelling, and B. Dabrowski, *Phys. Rev. Lett.* **73**, 3302 (1994)
- [13] D. H. Lu, M. Schmidt, T. R. Cummins, S. Schuppler, F. Lichtenberg, and J. G. Bednorz, *Phys. Rev. Lett.* **76**, 4845 (1996)
- [14] V. Khodel and V. Shaginyan, *JETP Lett.* **51**, 553 (1990)
- [15] P. Nozières, *J. Phys. I France* **2**, 443 (1992)
- [16] V. Y. Irkhin, A. A. Katanin, and M. I. Katsnelson, *Phys. Rev. Lett.* **89**, 076401 (2002)
- [17] D. Yudin, D. Hirschmeier, H. Hafermann, O. Eriksson, A. I. Lichtenstein, and M. I. Katsnelson, *Phys. Rev. Lett.* **112**, 070403 (2014)
- [18] J. Bok and J. Bouvier, *J. Supercond. Nov. Magn.* **25**, 657 (2012)
- [19] R. Nandkishore, L. S. Levitov, and A. V. Chubukov, *Nat. Phys.* **8**, 158 (2012)
- [20] M. L. Kiesel, C. Platt, W. Hanke, D. A. Abanin, and R. Thomale, *Phys. Rev. B* **86**, 020507 (2012)
- [21] C. Riedl, C. Coletti, T. Iwasaki, A. A. Zakharov, and U. Starke, *Phys. Rev. Lett.* **103**, 246804 (2009)
- [22] I. Gierz, T. Suzuki, R. T. Weitz, D. S. Lee, B. Krauss, C. Riedl, U. Starke, H. Höchst, J. H. Smet, C. R. Ast, and K. Kern, *Phys. Rev. B* **81**, 235408 (2010)



- [23] S. Forti, A. Stöhr, A. A. Zakharov, C. Coletti, K. V. Emtsev, and U. Starke, *2D Mater.* **3**, 035003 (2016)
- [24] J. Baringhaus, A. Stoehr, S. Forti, U. Starke, and C. Tegenkamp, *Sci. Rep.* **5** (2015)
- [25] See supplementary information for details on graphene growth, intercalation, experimental techniques, further characterization, ARPES raw data and DFT and FLEX which includes Refs. [40–52] URL `willbeinserted`
- [26] J. P. Perdew, K. Burke, and M. Ernzerhof, *Phys. Rev. Lett.* **77**, 3865 (1996)
- [27] G. Kresse and J. Hafner, *J. Phys.: Condens. Matter* **6**, 8245 (1994)
- [28] P. E. Blöchl, *Phys. Rev. B* **50**, 17953 (1994)
- [29] G. Kresse and D. Joubert, *Phys. Rev. B* **59**, 1758 (1999)
- [30] N. Bickers and D. Scalapino, *Ann. Phys.* **193**, 206 (1989)
- [31] Two different photon energies were used (30 eV and 100 eV) to access both the inner  $\pi^*$  band and the band course up to the outer  $\bar{K}'$  (see [25] for details and the original data sets).
- [32] J. M. Luttinger, *Phys. Rev.* **119**, 1153 (1960)
- [33] The electron density is derived from the difference between the area of the entire BZ and the hole pocket.
- [34] K. F. Mak, F. H. da Jornada, K. He, J. Deslippe, N. Petrone, J. Hone, J. Shan, S. G. Louie, and T. F. Heinz, *Phys. Rev. Lett.* **112**, 207401 (2014)
- [35] A. S. Mishchenko, N. V. Prokof'ev, A. Sakamoto, and B. V. Svistunov, *Phys. Rev. B* **62**, 6317 (2000)
- [36] A. V. Fedorov, N. I. Verbitskiy, D. Haberer, C. Struzzi, L. Petaccia, D. Usachov, O. Y. Vilkov, D. V. Vyalikh, J. Fink, M. Knupfer, B. Büchner, and A. Grüneis, *Nat. Commun.* **5**, 3257 (2014)
- [37] 1 ML is defined as a one atom thick layer of the (0001) plane of Gd.
- [38] B. E. Sernelius, *Phys. Rev. B* **91**, 045402 (2015)
- [39] U. A. Schröder, M. Petrović, T. Gerber, A. J. Martínez-Galera, E. Grånäs, M. A. Arman, C. Herbig, J. Schnadt, M. Kralj, J. Knudsen, and T. Michely, *2D Mater.* **4**, 015013 (2017)
- [40] C. Berger, Z. Song, T. Li, X. Li, A. Y. Ogbazghi, R. Feng, Z. Dai, A. N. Marchenkov, E. H. Conrad, P. N. First, and W. A. de Heer, *J. Phys. Chem. B* **108**, 19912 (2004)
- [41] T. Ohta, A. Bostwick, T. Seyller, K. Horn, and E. Rotenberg, *Science* **313**, 951 (2006)
- [42] C. Riedl, U. Starke, J. Bernhardt, M. Franke, and K. Heinz, *Phys. Rev. B* **76**, 245406 (2007)
- [43] K. V. Emtsev, F. Speck, T. Seyller, L. Ley, and J. D. Riley, *Phys. Rev. B* **77**, 155303 (2008)
- [44] C. Riedl, A. A. Zakharov, and U. Starke, *Appl. Phys. Lett.* **93**, 033106 (2008)
- [45] K. V. Emtsev, A. Bostwick, K. Horn, J. Jobst, G. L. Kellogg, L. Ley, J. L. McChesney, T. Ohta, S. A. Reshanov, J. Röhr, E. Rotenberg, A. K. Schmid, D. Waldmann, H. B. Weber, and T. Seyller, *Nat. Mater.* **8**, 203 (2009)
- [46] S. Forti and U. Starke, *J. Phys. D: Appl. Phys.* **47**, 094013 (2014)
- [47] M. Ostler, F. Speck, M. Gick, and T. Seyller, *Phys. Stat. Sol. (b)* **247**, 2924 (2010)
- [48] I. Gierz, J. Henk, H. Höchst, C. R. Ast, and K. Kern, *Phys. Rev. B* **83**, 121408 (2011)
- [49] V. I. Anisimov, F. Aryasetiawan, and A. I. Lichtenstein, *J. Phys.: Condens. Matter* **9**, 767 (1997)
- [50] P. Larson, W. R. L. Lambrecht, A. Chantis, and M. van Schilfhaarde, *Phys. Rev. B* **75**, 045114 (2007)
- [51] P. V. C. Medeiros, S. Stafström, and J. Björk, *Phys. Rev. B* **89**, 041407 (2014)
- [52] P. V. C. Medeiros, S. S. Tsirkin, S. Stafström, and J. Björk, *Phys. Rev. B* **91**, 041116 (2015)

# Supplementary information to 'Introducing strong correlation effects into graphene by gadolinium intercalation'

S. Link,<sup>1</sup> S. Forti,<sup>1,\*</sup> A. Stöhr,<sup>1</sup> K. Küster,<sup>1</sup> M. Rösner,<sup>2,3,4</sup> D. Hirschmeier,<sup>5</sup> C. Chen,<sup>6</sup> J. Avila,<sup>6</sup> M.C. Asensio,<sup>7</sup> A.A. Zakharov,<sup>8</sup> T.O. Wehling,<sup>2</sup> A.I. Lichtenstein,<sup>5</sup> M.I. Katsnelson,<sup>4</sup> and U. Starke<sup>1,†</sup>

<sup>1</sup>*Max-Planck-Institut für Festkörperforschung,  
Heisenbergstr. 1, D-70569 Stuttgart, Germany*

<sup>2</sup>*Institute for Theoretical Physics, Bremen Center for Computational Materials Science,  
University of Bremen Otto-Hahn-Allee 1, 28359 Bremen, Germany*

<sup>3</sup>*Department of Physics and Astronomy,  
University of Southern California, Los Angeles, CA 90089-0484, USA*

<sup>4</sup>*Radboud University, Institute for Molecules & Materials,  
Heijendaalseweg 135, 6525 AJ Nijmegen, Netherlands*

<sup>5</sup>*Universität Hamburg, Institut für Theoretische Physik, D-20355 Hamburg, Germany*

<sup>6</sup>*Synchrotron SOLEIL and Université Paris Saclay,  
Orme des Merisiers, Saint-Aubin-BP 48, 91192 Gif sur Yvette, France*

<sup>7</sup>*Madrid Institute of Materials Science (ICMM),  
Spanish Scientific Research Council (CSIC),  
Cantoblanco, E-28049 Madrid - SPAIN*

<sup>8</sup>*MAX IV Laboratory, Lund University,  
Fotongatan 2, 22484 Lund, Sweden*

PACS numbers:

# GRAPHENE GROWTH ON SiC(0001): BUFFER LAYER (ZLG) AND QUASI-FREE STANDING GRAPHENE

Epitaxial graphene on SiC(0001) is commonly prepared by means of silicon sublimation via annealing of the SiC substrate [1–3]. An initial carbon layer develops – well ordered in a  $(6\sqrt{3}\times 6\sqrt{3})R30^\circ$  superstructure on the SiC(0001) substrate – which structurally is composed of the typical carbon honeycomb lattice found in graphene. However, about one third of the carbon atoms are still covalently bound to the topmost silicon atoms in the substrate so that the delocalized  $\pi$  band system cannot develop [4, 5]. This initial carbon layer is called buffer layer or zero-layer graphene (ZLG). The covalent bonding situation is sketched in Fig. S1(a) with the covalent bonds between Si and C across the interface and dangling bonds (DB) on the remaining Si atoms indicated. We note that this bonding induces a strong buckling in the graphitic layer and leads to a very distinct and intense quasi- $(6\times 6)$ -SiC(0001) diffraction pattern [3]. By further annealing of the SiC sample a second carbon layer is formed, which in turn assumes the role of the buffer layer. The initial ZLG transforms into a real graphene layer on top with fully developed  $\pi$  bands and the system is then called monolayer graphene (MLG) (see Fig. S1(b) for a side view sketch). In the present study, ZLG samples with homogeneous coverage were prepared on 6H-SiC(0001) (on-axis, n-doped, purchased from SiCrystal GmbH) by annealing in a home-built RF-furnace in Ar atmosphere, which results in a superb homogeneity on a waver scale [6–8]. Atomic force microscopy (AFM), low energy electron diffraction (LEED) and X-ray photoelectron spectroscopy (XPS) were used to control the quality of the growth. The ZLG carbon layer (which does not display  $\pi$  bands)

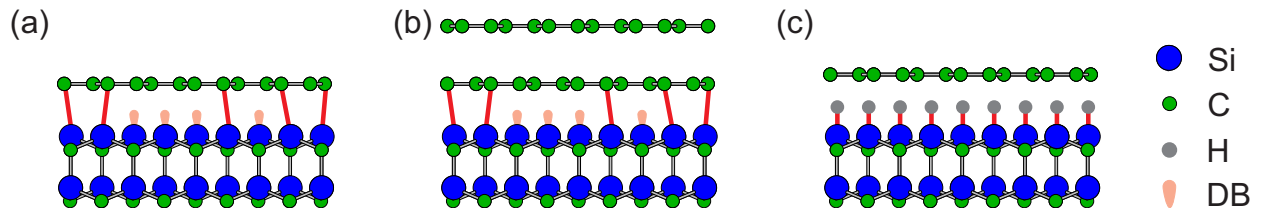


FIG. S1: Model sketches of epitaxial graphene on SiC(0001) in side view: (a) Buffer layer or zero-layer graphene (ZLG) with covalent Si-C interface bonds and substrate Si dangling bonds (DB), (b) Monolayer graphene (MLG) composed of one ZLG at the SiC interface and one van-der Waals bound graphene layer on top and (c) quasi-free standing graphene after hydrogen intercalation.



can be decoupled from the SiC substrate by an intercalated atomic layer, as first shown for hydrogen intercalation [9]. The covalent bonds at the ZLG interface are broken and all Si atoms in the topmost substrate layer are saturated by hydrogen atoms. Effectively in this way, a quasi-free standing graphene monolayer (QFMLG) is obtained as depicted in the sketch in Fig. S1(c) and this QFMLG now has sharp monolayer  $\pi$  bands [9].

## INTERCALATION METHOD AND EXPERIMENTAL TECHNIQUES

In the present study, decoupling by intercalation could also be achieved using a Gd layer. In detail, Gd was evaporated onto the samples using a commercial e-beam evaporator. During evaporation, the sample temperature is held at 800 °C. After this step, the sample is fully intercalated with Gd, which was verified by means of XPS, LEED and angle-resolved photoelectron spectroscopy (ARPES). With the temperature of only 800 °C during the intercalation process, it is ensured, that no further Si sublimation takes place and no additional carbon layer is grown [3]. Yet, the characteristic  $(13\sqrt{3}\times 13\sqrt{3})R30^\circ$ -graphene structure does not yet develop. To achieve this superior order, the samples had to be heated for a very short time (about 5 s) to about 1200 °C. The spectroscopic footprints of the intercalated system are not affected by this treatment, i.e. ARPES and XPS characterization is unchanged, so that it is clear that we still deal with a quasi-free monolayer system. After this procedure, no degeneration could be detected when heating up to temperatures higher than 1000 °C. Also, no degeneration in the samples can be found when keeping the samples in UHV conditions ( $p < 1 \times 10^{-8}$  mbar) on a timescale of weeks. Direct exposure to air, however, leads to notable degeneration (see below). In order to prevent degeneration during transport to the synchrotron facilities for the ARPES measurements shown, these samples were covered with about 100 nm of Bi which in turn was removed by heating to temperatures higher than 700 °C in the beamlines' vacuum facilities. Comparative measurements by means of XPS, LEED and ARPES in the home laboratory confirmed the validity of this treatment, and indeed no differences to the pristine intercalated samples were found.

## ARPES RAW DATA

The extended ARPES dispersion plot shown in Fig. 1(c) of the main text had to be concatenated from two measurements with different photon energy for two reasons: On the one hand, the high energy of 100 eV is necessary to allow the full scan along the  $\overline{\text{KMK}}'$  line since the emission angle for the  $\overline{\text{K}}'$  point would be too large at lower photon energies. On the other hand, the low energy of 30 eV is needed for the region around the  $\overline{\text{K}}$  point

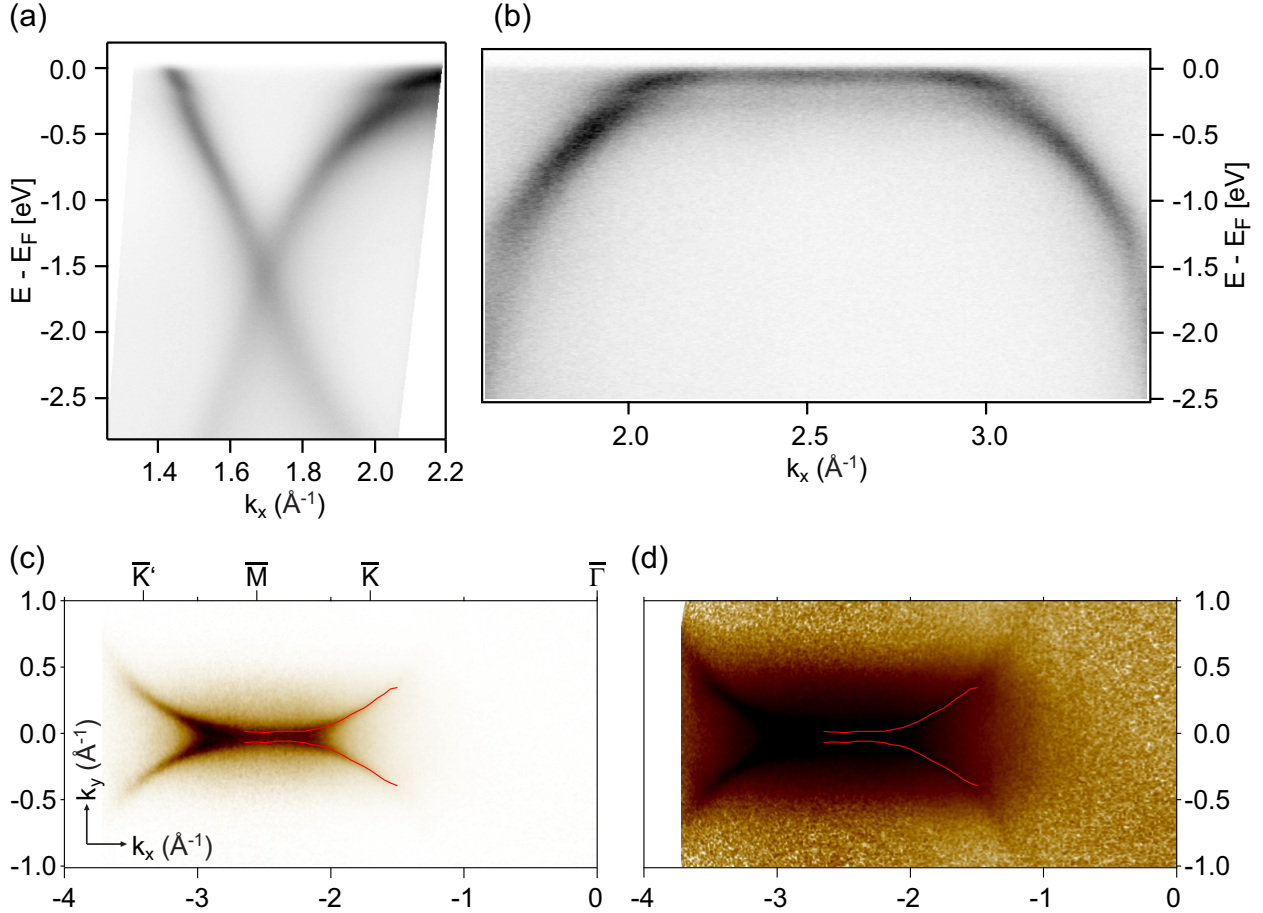


FIG. S2: ARPES raw data of the Gd intercalated ZLG system: (a) Dispersion across the  $\overline{\text{K}}$  point projected along the  $\overline{\text{K}\overline{\text{K}}}$  direction measured with 30 eV photon energy. (b) Dispersion along the  $\overline{\text{KMK}}'$  line measured with 100 eV photon energy. (c) Fermi surface from the  $\overline{\Gamma}$  point in the first BZ up to the  $\overline{\text{K}}$  point in the repeated BZ and (d) the same data set plotted with enhanced contrast and logarithmic intensity scale. Measurement taken with 90 eV photon energy, emission angle scan range of  $55^\circ$ .

in order to access both, the  $\pi$  band and  $\pi^*$  band branches, the latter of which would be suppressed at 100 eV photon energy due to matrix element effects [10]. For clarity, we display the raw data used for Fig. 1(c) in Fig. S2(a and b). The two data sets are acquired from the same sample in the same preparation run (beamline Antares at Soleil). Figure 1(d) of the main text presents a symmetrized FS taken with 90 eV photon energy. The FS is extracted from an exhaustive scan of ARPES dispersion slices covering the first BZ from the  $\bar{\Gamma}$  point to the  $\bar{K}$  point and continuing along the border of the repeated BZ along the  $\overline{KMK'}$  line, thus covering a large range of emission angles (beamline I4 at MAX-Lab). In Fig. 1(d), the data is repeated in  $60^\circ$  rotation, so that the course of the  $\pi$  bands can be observed. We display the raw Fermi surface data extracted from this measurement in Fig. S2(c) together with the fitted band course at the Fermi energy (The Fermi surface points were evaluated individually from momentum distribution curves extracted perpendicular to the  $\overline{KMK'}$  line and symmetry repeated around the first BZ in Fig. 1(d)). Notably, spectral weight is completely absent inside the  $\pi$  band ring in the first BZ, and in particular in the region of the  $\bar{\Gamma}$  point indicating that no interlayer Gd band is present in this system. This can be seen in a contrast enhanced display of the same data set with logarithmic intensity scale in Fig. S2(d). We note again, that due to matrix element effects, the  $\pi^*$  band intensity is strongly suppressed at the photon energy utilized in this measurement [10]. All ARPES data were acquired with the sample liq. N<sub>2</sub> cooled ( $\approx 90$ K) and using nominally linear polarization (p).

## FURTHER EXPERIMENTAL CHARACTERIZATION

To shine light on the state of the Gd intercalated samples we firstly performed XPS measurements using Al K $_{\alpha}$  radiation at normal and grazing emission for different surface sensitivity. Fig. S3(a) shows the spectra related to the C 1s, Si 2p and Gd 3d<sub>5/2</sub> core levels respectively. The relative intensity is normalized to the Gd 3d peak at  $0^\circ$  and  $60^\circ$  respectively. It is well visible, that the Si 2p component as well as the C 1s component at 282.7eV binding energy are suppressed when increasing the emission angle. The relative intensity of the C1s component at about 285eV binding energy, however, increases when increasing the emission angle. The LEEM micrograph shown in Fig. S3(b) displays a completely homogeneous surface without any Gd clusters on top. The only contrast visible is related

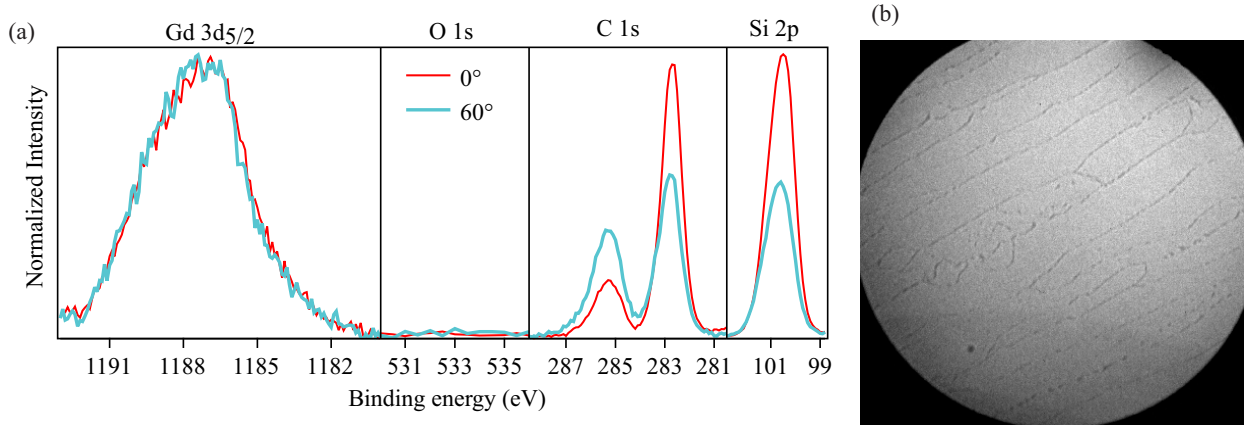


FIG. S3: (a) XPS measurements in the binding energy regions of the Gd 3d, O 1s, C 1s, Si 2p acquired with Al  $K_{\alpha}$  radiation at different emission angles. (b) LEEM micrograph of a Gd intercalated ZLG sample with a field of view of  $25 \mu\text{m}$  measured with electron energy 1.2 eV.

to step edges in the SiC substrate, which is intrinsic to epitaxial graphene on SiC(0001). Considering the simplicity of the initial ZLG system, i.e. one graphitic layer on top of the SiC, this information is sufficient to conclude that the Gd is sandwiched by the SiC and the graphitic layer. It has to be noted, that no O 1s component appears for these samples when safekeeping under UHV conditions. This is also indicative for the sandwich configuration, as the graphene layer protects the Gd from oxidation by residual gas in the vacuum chamber. Direct exposure to air induces degradation. As visible in the ARPES cuts in Fig. S4(a) (photon energy 60 eV, beamline I4 at MAX-Lab), the doping level gets strongly reduced, so that the Dirac point is located at about 0.5 eV, whereas it is about 1.6 eV in the pristine intercalated samples. In XPS a strong O 1s can then be found. This cannot be reversed by mild outgasing in UHV to remove adsorbed water or oxygen. One can therefore conclude that under air exposure, oxygen or water migrates beneath the graphene layer in these samples and presumably reacts chemically with the Gd. The XPS measurements in Fig. S4(b) as well as Fig. 3(c,e) were taken at beamline I311 at MAX-Lab.

## DENSITY FUNCTIONAL THEORY

The density functional theory (DFT) calculations were performed within the generalized gradient approximation (GGA) [11] using the Vienna Ab Initio Simulation Package (VASP)

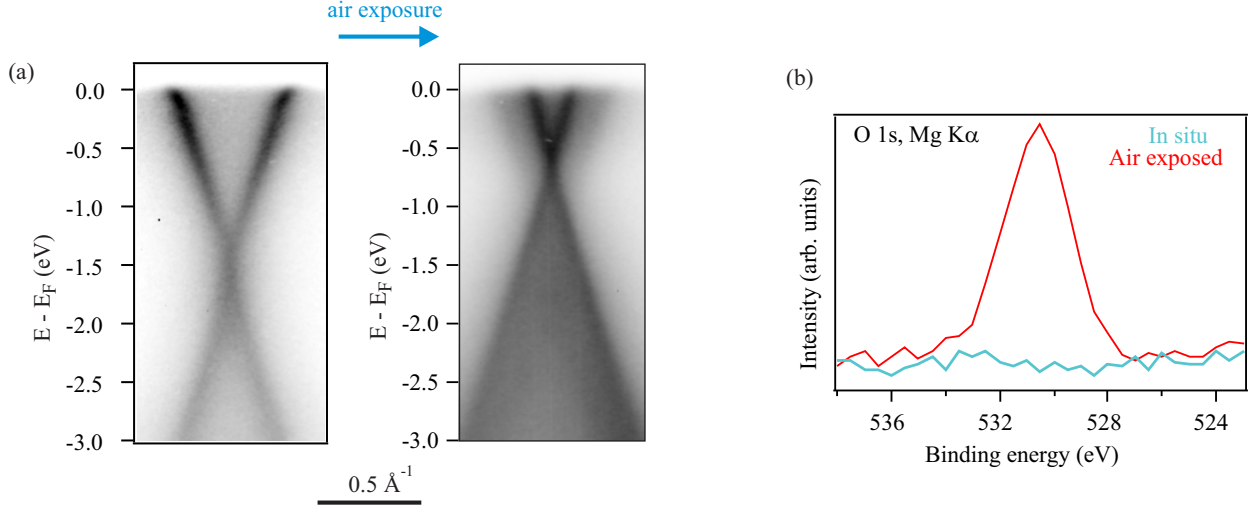


FIG. S4: (a) ARPES on the  $\pi$  bands before and after air exposure. (b) XPS in the region of the O 1s level before and after air exposure.

[12] and the projector augmented wave (PAW) [13, 14] basis sets. We account for the strong local Coulomb interactions of the Gd 4f-electrons within the GGA+U approach using the Coulomb parameters  $U = 7$  eV and  $J = 1$  eV, which have been shown to be well suited to describe rare earth systems [15, 16]. We considered Gd adsorbed on graphene in the  $(\sqrt{3} \times \sqrt{3})R30^\circ$  structure as shown in Fig. 3 (c) of the manuscript. While the graphene lattice constant was fixed to a value of  $a_0 \approx 2.48$  Å, the Gd  $z$  position was relaxed until forces were below  $0.001$  eV Å $^{-1}$  resulting in a  $z$  distance of  $a_z \approx 2.23$  Å. After finding the self-consistent ground state, we use the BandUP code [17, 18] to unfold the spin-resolved band structure of the  $(\sqrt{3} \times \sqrt{3})R30^\circ$  unit cell to the primitive cell of graphene.

## FLUCTUATING EXCHANGE APPROXIMATION

The spectral function shown in panel (b) of Fig. 4 was calculated using the fluctuating exchange approximation (FLEX) [19], which will be outlined in this section. Starting with the partition function in the path integral representation

$$\mathcal{Z} = \int D[c^*, c] e^{-S[c^*, c]}, \quad (1)$$

where the action depends on the complex Grassmann fields  $c^*$  and  $c$ , representing the respective creation and annihilation of fermions, we investigate electronic correlation effects

in doped graphene by considering the Hubbard model on the bipartite honeycomb lattice which can be written by

$$S = S_0 + V = - \sum_{ij\sigma\nu} c_{i\sigma\nu}^* [(i\nu_n + \mu)\delta_{ij} - \epsilon_{\mathbf{k}}^{ij}] c_{j\sigma\nu} + U \sum_{j\nu\nu'\Omega} c_{j\nu}^{*\uparrow} c_{j\nu+\Omega}^\uparrow c_{j\nu'+\Omega}^{*\downarrow} c_{j\nu'}^\downarrow, \quad (2)$$

where  $\sigma = \uparrow, \downarrow$  is the spin projection,  $\nu_n = (2n + 1)\pi T$  the  $n$ -th fermionic Matsubara frequency,  $\Omega = 2n\pi T$ , the  $n$ -th bosonic Matsubara frequency,  $\mathbf{k}$  the lattice momentum and the sum is taken over the four momentum  $\nu = (i\nu_n, \mathbf{k})$ . Latin letters  $i, j$  represent the two sublattices of the honeycomb lattice. Note that indices being super or subscript does not hold any further meaning here and in the following and we will only use one or the other for the sake of readability. The model parameters are the chemical potential  $\mu$ , temperature  $T$ , Hubbard interaction  $U$  and nearest-neighbour hopping amplitude  $t$ . The latter enters the tight-binding dispersion  $\epsilon_{\mathbf{k}}$ , which can be written as a  $2 \times 2$  matrix in sublattice degrees of freedom

$$\epsilon_{\mathbf{k}} = \begin{pmatrix} 0 & -t f_{\mathbf{k}} \\ -t f_{\mathbf{k}}^* & 0 \end{pmatrix}, \quad (3)$$

where  $f_{\mathbf{k}} = e^{-i(\frac{a}{\sqrt{3}}k_y)} + 2e^{i(\frac{a}{2\sqrt{3}}k_y)} \cos(\frac{a}{2}k_x)$  with  $a$  being the lattice constant. We set the main diagonal to zero, as we restrict ourselves to nearest-neighbour hopping. Note that within our model the interaction is restricted to a local density-density interaction and we ignore the Coulomb repulsion between electrons residing on different sites.

Theoretically the ARPES data correspond to the energy and momentum resolved spectral function given by the imaginary part of the retarded Greens function  $A_{\mathbf{k},\omega} = \frac{-1}{\pi} \text{Im} G_{\mathbf{k},\omega+i0^+}$ , where  $\omega$  labels real frequencies. Correlation effects between electrons enter the Greens function through the self-energy  $\Sigma_\nu$  via the Dyson equation

$$G_\nu = \begin{pmatrix} \nu + \mu - \Sigma_\nu^{00} & -\epsilon_{\mathbf{k}} - \Sigma_\nu^{01} \\ -\epsilon_{\mathbf{k}}^* - \Sigma_\nu^{10} & \nu + \mu - \Sigma_\nu^{11} \end{pmatrix}^{-1}. \quad (4)$$

Therefore our problem boils down to finding an appropriate approximation to the self-energy. We expect that correlation effects from antiferromagnetic fluctuations are responsible for the band flatting, which can be approximated by ladder diagrams of particle-hole type. The corresponding self-energy can be written in terms of these diagrams using the Schwinger-Dyson



equation (SDE), which can be derived from the equation of motion for the Greens function and the Dyson equation. In the language of the coherent state path integral formalism the SDE can be obtained from

$$\Sigma_{\alpha\beta}G_{\beta\gamma} = \left\langle c_{\gamma}^* \frac{\partial V}{\partial c_{\alpha}^*} \right\rangle, \quad (5)$$

where greek letters represent general single-particle degrees of freedom. Inserting the interaction  $V$  from the second line of Eq. (2), the SDE for the problem at hand is

$$\Sigma_{\nu}^{\sigma ij} = U \langle n_{\bar{\sigma}} \rangle \delta_{ij} - U \sum_{\nu'\omega,acd} G_{\nu+\omega}^{\sigma ia} \Gamma^{\bar{\sigma}\bar{\sigma}\sigma\sigma,ajcd} G_{\nu'+\omega}^{\bar{\sigma} di} G_{\nu'}^{\bar{\sigma} ic}, \quad (6)$$

where  $\Gamma$  is the full two-particle vertex representing all connected diagrammatic contributions to the two-particle Greens function and  $\bar{\sigma} = -\sigma$ . Note that we are only considering the paramagnetic case, where all quantities are invariant under rotation of spins. The two-particle Greens function is defined as

$$G_{\nu\nu'\Omega}^{(2)abcd} = \frac{1}{\mathcal{Z}} \int D[c^*, c] c_{\nu+\omega}^a c_{\nu}^{*b} c_{\nu'}^c c_{\nu'+\omega}^{*d} e^{-S[c^*, c]} \quad (7)$$

and is related to  $\Gamma$  via

$$\begin{aligned} G_{\nu\nu'\Omega}^{(2)abcd} &= G_{\nu+\Omega}^{ab} G_{\nu'+\Omega}^{cd} \delta_{\Omega 0} - G_{\nu+\Omega}^{ad} G_{\nu'+\Omega}^{cb} \delta_{\nu\nu'} \\ &+ G_{\nu+\Omega}^{aa'} G_{\nu}^{cc'} \Gamma_{\nu\nu'\Omega}^{a'b'c'd'} G_{\nu'}^{b'b} G_{\nu'+\Omega}^{d'd}, \end{aligned} \quad (8)$$

where the last equation defines the two-particle vertex. Diagrammatic contributions to the two-particle vertex fall into one of two groups, those which are fully irreducible and those which are reducible with respect to one of three channels. Those channels are the particle-particle (pp), the vertical (v) and the horizontal (h) particle-hole channel. Reducibility with respect to one of these channels means, that a diagram can be split into two diagrams by respectively cutting a particle-particle, vertical particle-hole or horizontal particle-hole pair propagator. The full two-particle vertex can thus be written as

$$\Gamma = \Gamma_{firr} + \Gamma_{red}^{(p)} + \Gamma_{red}^{(v)} + \Gamma_{red}^{(h)}, \quad (9)$$

where  $\Gamma_{firr}$  represents all fully irreducible contributions and  $\Gamma_{red}^{(\alpha)}$  represents the contributions reducible with respect to channel  $\alpha = p, v, h$ . As neither the self-energy nor the two-particle vertex are known exactly for the problem defined by Eqs. (1)-(2), sensible approximations, that is, suitable to qualitatively describe the physical phenomenon of interest, have to be

employed. In this work an approximation to the self-energy is obtained from the SDE and a suitable approximation to the vertex which is threefold:

- The fully irreducible two-particle vertex is approximated by the bare interaction  $\Gamma_{firr} \approx U$ .
- Only reducible two-particle diagrams in either the vertical or the horizontal particle-hole channel are taken into account, whereas particle-particle reducible contributions are neglected  $\Gamma_{red}^{(p)} = 0$ .
- All reducible contributions are obtained from the solution of the Bethe-Salpeter equation in the respective channel  $\Gamma^{(\alpha)}$ , where the irreducible diagrams with respect to either channel are approximated again by the bare interaction  $U$  and the corresponding reducible contribution is then  $\Gamma_{red}^{(\alpha)} = \Gamma^{(\alpha)} - U$ .

Thus Eq. (9) becomes  $\Gamma = \Gamma^{(h)} + \Gamma^{(v)} - U$ , where the indices  $v, h$  represent the vertical and horizontal particle-hole channel respectively. The  $\Gamma^{(\alpha)}$  contributions to the SDE are now given by ladder diagrams of the form

$$\Gamma_{\uparrow\uparrow\downarrow\downarrow}^{(h)ijj} = \begin{array}{c} \uparrow i \quad \downarrow i \\ \diagdown \quad \diagup \\ \text{---} \\ \diagup \quad \diagdown \\ \uparrow i \quad \downarrow i \end{array} + \begin{array}{c} \uparrow i \quad \downarrow i \\ \diagdown \quad \diagup \\ \text{---} \circ \text{---} \\ \diagup \quad \diagdown \\ \uparrow i \quad \downarrow i \end{array} + \dots \quad (10)$$

$$\Gamma_{\uparrow\uparrow\downarrow\downarrow}^{(v)ijj} = \begin{array}{c} \uparrow i \quad \downarrow i \\ \diagdown \quad \diagup \\ \text{---} \\ \diagup \quad \diagdown \\ \uparrow i \quad \downarrow i \end{array} + \begin{array}{c} \uparrow i \downarrow \quad \downarrow i \\ \diagdown \quad \diagup \\ \text{---} \\ \diagup \quad \diagdown \\ \uparrow j \downarrow \quad \downarrow j \end{array} + \begin{array}{c} \uparrow i \downarrow \quad \downarrow i \\ \diagdown \quad \diagup \\ \text{---} \\ \diagup \quad \diagdown \\ \uparrow j \downarrow \quad \downarrow j \end{array} + \dots \quad (11)$$

Note that the restriction to ladder diagrams only generates reducible vertex contributions with sublattice structure  $\Gamma^{ijkl} = \Gamma^{ijj} \delta_{ij} \delta_{kl}$ . While the vertex components contributing to the SDE come from both the vertical and horizontal channel and have spin structure  $\uparrow\uparrow\downarrow\downarrow$ , it is possible to evaluate the SDE using only the horizontal channel by exploiting symmetries. First note that, up to a sign, Eq. (11) is equivalent to

$$\Gamma_{\uparrow\downarrow\downarrow\uparrow}^{(h)ijji} = \begin{array}{c} \uparrow i \quad \uparrow i \\ \text{---} \\ \downarrow i \quad \downarrow i \end{array} + \begin{array}{c} \uparrow i \quad \uparrow \quad \uparrow j \\ \text{---} \\ \downarrow i \quad \downarrow \quad \downarrow j \end{array} + \dots \quad (12)$$

where even as well as odd orders contribute. While the odd orders are, again up to a sign, equivalent to the contributions from Eq. (10) the even orders are equivalent to the diagrams given by

$$\Gamma_{\uparrow\uparrow\uparrow\uparrow}^{(h)ijjj} = \begin{array}{c} \nearrow \uparrow i \\ \text{---} \circlearrowleft \text{---} \\ \searrow \uparrow j \\ \uparrow i \quad \downarrow \quad \uparrow j \\ \nwarrow \uparrow i \end{array} + \dots \quad (13)$$

Hence  $\Gamma^{\uparrow\uparrow\downarrow\downarrow} = 2\Gamma^{(h)\uparrow\uparrow\downarrow\downarrow} - \Gamma^{(h)\uparrow\uparrow\uparrow\uparrow} - U$ . The dots at the end of Eqs. (10)-(13) indicate the summation of an infinite power series in  $U$  and yield

$$\Gamma^{(h)\uparrow\uparrow\downarrow\downarrow} = U \sum_n (U^2 \chi_\omega^2)^n = U (1 - U^2 \chi_\omega^2)^{-1} \quad (14)$$

$$\Gamma^{(h)\uparrow\uparrow\uparrow\uparrow} = -U^2 \chi_\omega \sum_n (U^2 \chi_\omega^2)^n = -U^2 \chi (1 - U^2 \chi_\omega^2)^{-1} \quad (15)$$

$$\Gamma^{(h)\uparrow\downarrow\downarrow\uparrow} = -U \sum_n (U \chi_\omega)^n = -U (1 - U \chi_\omega)^{-1} \quad (16)$$

$$\chi_\omega = \frac{1}{N} \sum_\nu G_{\nu+\omega} G_\nu, \quad (17)$$

and it is easy to check that  $\Gamma^{(h)\uparrow\downarrow\downarrow\uparrow} = \Gamma^{(h)\uparrow\uparrow\uparrow\uparrow} - \Gamma^{(h)\uparrow\uparrow\downarrow\downarrow}$ . Note that the dependence on sublattice degrees of freedom was ignored in the equations above. However it can be easily restored by assigning matrix value to the left and right hand side of the equations and respectively replace the interaction  $U$  and the particle-hole bubble with  $2 \times 2$  matrices in sublattice space according to

$$\hat{U} = U \mathbf{1} \quad (18)$$

$$\hat{\chi} = \begin{pmatrix} \chi^{00} & \chi^{01} \\ \chi^{10} & \chi^{11} \end{pmatrix} \quad (19)$$

$$\chi_\omega^{ab} = \frac{1}{N} \sum_\nu G_{\nu+\omega}^{ab} G_\nu^{ba} \quad (20)$$

Thus dropping the spin dependence one ends up with the final expression for the self-energy

$$\Sigma_\nu^{ij} = U \langle n_{\bar{\sigma}} \rangle \delta_{ij} - U \sum_{\omega, k} G_{\nu+\omega}^{ij} \Gamma^{jjkk} \chi_\omega^{ki}, \quad (21)$$

where  $\Gamma^{jjkk}$  is given by the  $j, k$  component of matrix

$$\hat{\Gamma} = \frac{3}{2} U (1 + U \hat{\chi})^{-1} + \frac{U}{2} (1 - U \hat{\chi})^{-1} \quad (22)$$

Using the thus obtained self-energy in the Dyson equation (4) we gain the renormalized Greens function  $G_\nu$ , from which we obtain the spectral function shown in Fig. 4 (b) of the main text.

All equations are evaluated using the bare propagators.

---

\* present address: Center for Nanotechnology Innovation CNI@NEST, Piazza San Silvestro 12, 56127 Pisa, Italy

† To whom correspondence should be addressed:

Email: [u.starke@fkf.mpg.de](mailto:u.starke@fkf.mpg.de);

Electronic address: <http://www.fkf.mpg.de/ga>

- [1] C. Berger, Z. Song, T. Li, X. Li, A. Y. Ogbazghi, R. Feng, Z. Dai, A. N. Marchenkov, E. H. Conrad, P. N. First, and W. A. de Heer, *J. Phys. Chem. B* **108**, 19912 (2004)
- [2] T. Ohta, A. Bostwick, T. Seyller, K. Horn, and E. Rotenberg, *Science* **313**, 951 (2006)
- [3] C. Riedl, U. Starke, J. Bernhardt, M. Franke, and K. Heinz, *Phys. Rev. B* **76**, 245406 (2007)
- [4] K. V. Emtsev, F. Speck, T. Seyller, L. Ley, and J. D. Riley, *Phys. Rev. B* **77**, 155303 (2008)
- [5] C. Riedl, A. A. Zakharov, and U. Starke, *Appl. Phys. Lett.* **93**, 033106 (2008)
- [6] K. V. Emtsev, A. Bostwick, K. Horn, J. Jobst, G. L. Kellogg, L. Ley, J. L. McChesney, T. Ohta, S. A. Reshanov, J. Röhrl, E. Rotenberg, A. K. Schmid, D. Waldmann, H. B. Weber, and T. Seyller, *Nat. Mater.* **8**, 203 (2009)
- [7] S. Forti and U. Starke, *J. Phys. D: Appl. Phys.* **47**, 094013 (2014)
- [8] M. Ostler, F. Speck, M. Gick, and T. Seyller, *Phys. Stat. Sol. (b)* **247**, 2924 (2010)
- [9] C. Riedl, C. Coletti, T. Iwasaki, A. A. Zakharov, and U. Starke, *Phys. Rev. Lett.* **103**, 246804 (2009)
- [10] I. Gierz, J. Henk, H. Höchst, C. R. Ast, and K. Kern, *Phys. Rev. B* **83**, 121408 (2011)
- [11] J. P. Perdew, K. Burke, and M. Ernzerhof, *Phys. Rev. Lett.* **77**, 3865 (1996)
- [12] G. Kresse and J. Hafner, *J. Phys.: Condens. Matter* **6**, 8245 (1994)
- [13] P. E. Blöchl, *Phys. Rev. B* **50**, 17953 (1994)
- [14] G. Kresse and D. Joubert, *Phys. Rev. B* **59**, 1758 (1999)
- [15] V. I. Anisimov, F. Aryasetiawan, and A. I. Lichtenstein, *J. Phys.: Condens. Matter* **9**, 767 (1997)

- [16] P. Larson, W. R. L. Lambrecht, A. Chantis, and M. van Schilfgaarde, Phys. Rev. B **75**, 045114 (2007)
- [17] P. V. C. Medeiros, S. Stafström, and J. Björk, Phys. Rev. B **89**, 041407 (2014)
- [18] P. V. C. Medeiros, S. S. Tsirkin, S. Stafström, and J. Björk, Phys. Rev. B **91**, 041116 (2015)
- [19] N. Bickers and D. Scalapino, Ann. Phys. **193**, 206 (1989)